Nature of ground states in one-dimensional electron-phonon Hubbard models at half filling

H. Bakrim[1,*] and C. Bourbonnais[1,†]

[1]*Regroupement Québecois sur les Matériaux de Pointe, Département de physique, Université de Sherbrooke, Sherbrooke, Québec, Canada, J1K-2R1*

(Dated: February 23, 2015)

The renormalization group technique is applied to one-dimensional electron-phonon Hubbard models at half-filling and zero temperature. For the Holstein-Hubbard model, the results of one-loop calculations are congruent with the phase diagram obtained by quantum Monte Carlo simulations in the $(U, g_{\rm ph})$ plane for the phonon-mediated interaction $g_{\rm ph}$ and the Coulomb interaction U. The incursion of an intermediate phase between a fully gapped charge-density-wave state and a Mott antiferromagnet is supported along with the growth of its size with the molecular phonon frequency ω_0. We find additional phases enfolding the base boundary of the intermediate phase. A Luttinger liquid line is found below some critical $U^* \approx g^*_{\rm ph}$, followed at larger $U \sim g_{\rm ph}$ by a narrow region of bond-order-wave ordering which is either charge or spin gapped depending on U. For the Peierls-Hubbard model, the region of the $(U, g_{\rm ph})$ plane with a fully gapped Peierls-bond-order-wave state shows a growing domination over the Mott gapped antiferromagnet as the Debye frequency ω_D decreases. A power law dependence $g_{\rm ph} \sim U^{2\eta}$ is found to map out the boundary between the two phases, whose exponent is in good agreement with the existing quantum Monte Carlo simulations performed when a finite nearest-neighbor repulsion term V is added to the Hubbard interaction.

PACS numbers: 71.10.Fd, 71.30.+h, 71.45.Lr

I. INTRODUCTION

In approaching the physics of highly correlated electron systems, we often come against experimental evidence for significant coupling between interacting electrons and lattice degrees of freedom of different kinds[1–3]. The fact that the electron-phonon coupling can play an important part besides the electron-electron interaction takes on particular importance in reduced dimensions where the intrinsically expanded range of electronic instabilities can be further broadened by the interplay between both interactions.[4–6]

In this matter one-dimensional (1D) models of interacting electrons coupled to a bosonic phonon field have been long considered as primary models to study the competing effects of Coulomb and retarded interactions on ordered phases at zero temperature. In the present work we shall be concerned with two models at half-filling that have been the focus of considerable attention in the past few decades, namely the 1D Holstein-Hubbard model (HH)[7,8] and the Su-Schrieffer-Heeger-Hubbard model[9] and its variant for optical phonons called for short the Peierls-Hubbard (PH) model[4,5,10].

The corresponding Hamiltonians can be introduced through the following common form in Fourier space,

$$\begin{aligned} H = &\sum_{k,\sigma} \varepsilon(k) c^\dagger_{k\sigma} c_{k\sigma} + \sum_q \omega_q \Big(b^\dagger_q b_q + \frac{1}{2} \Big) \\ &+ \frac{1}{\sqrt{L}} \sum_{k,q,\sigma} g(k,q) (b^\dagger_q + b_{-q}) c^\dagger_{k+q,\sigma} c_{k\sigma} \\ &+ \frac{U}{L} \sum_q n_{q\uparrow} n_{-q\downarrow} + \frac{1}{L} \sum_q V_q \, n_q n_{-q}, \end{aligned} \tag{1}$$

where $c^\dagger_{k\sigma}(c_{k\sigma})$ creates (annihilates) an electron of wave vector k and spin σ, and L is the number of lattice sites (the lattice distance $a = 1$). The electron spectrum is

$$\varepsilon(k) = -2t \cos k, \tag{2}$$

where t is the hopping amplitude. At half-filling the band is filled up to the Fermi points $\pm k_F = \pm\pi/2$.

In the case of the HH model, momentum independent intramolecular phonons of energy $\omega_q \equiv \omega_0$ ($\hbar = 1$), described by the creation (annihilation) phonon operators $b^\dagger_q(b_q)$ of wave vector q, are coupled to electrons through the momentum independent coupling constant

$$g(k,q) \equiv g_0, \qquad \text{(HH)} \tag{3}$$

where $g_0 > 0$.

For the Su-Schrieffer-Heeger model, the phonons belong to an acoustic branch of frequency,

$$\omega_q = \omega_D |\sin q/2|, \tag{4}$$

where ω_D corresponds to the Debye frequency for the zone boundary $q = \pi$ phonon, namely at twice the Fermi wave vector $2k_F$ for a half-filled band. Their coupling to electrons results from the modulation of the electron transfer integral by lattice vibrations which leads to the momentum-dependent coupling constant

$$g(k,q) = i g_D \sin \frac{q}{2} \cos\Big(k + \frac{q}{2}\Big) \tag{5}$$

where g_D is a constant proportional to the spatial derivative of the hopping integral t. Retaining only the coupling to $q = 2k_F$ phonons at the zone edge corresponds to the PH limit.

The Coulomb part of the Hamiltonian (1) is common to both models. It comprises the Hubbard and extended-Hubbard interactions U and V ($V_q = V\cos q$) between electrons on each site and nearest-neighbor sites. These are expressed in terms of the occupation number, $n_q = n_{q\uparrow} + n_{q\downarrow}$, where $n_{q\sigma} = \sum_k c^\dagger_{k+q,\sigma} c_{k\sigma}$.

The phase diagrams of both models have been the object of sustained interest during the last decades. To start with the half-filled HH model in the pure Hubbard limit at $V = 0$, many efforts have been devoted to clarifying its structure. Special emphasis has been put on the frontier separating the fully gapped (spin and charge) $2k_F$ site-centered charge-density-wave (CDW) and the charge (Mott) gapped $2k_F$ spin-density-wave (M-SDW) phases, namely when the amplitude of the phonon-mediated electron coupling

$$g_{\rm ph} = 2g_0^2/\omega_0, \qquad \text{(HH)}$$

becomes of the order of the local repulsion U.

The existence of an intermediate metallic state was predicted to occur long ago on the basis of real-space renormalization group arguments[11], but found to be absent in former world line Monte Carlo simulations[8] and two-cut off renormalization group analysis[12,13]. The presence of such a state was more recently supported by density matrix renormalization group (DMRG) and variational methods[14,15]. Its origin was thereafter extensively discussed from various approaches[16–21]. In particular, quantum Monte Carlo (QMC)[16,18,22] and further DMRG[23] calculations have corroborated its existence over a definite, ω_0-dependent region of the $(U, g_{\rm ph})$ plane. On more analytical grounds, the phase diagram of the HH model has been investigated by the functional RG (fRG) method at the one-loop level.[19] The frequency dependence of the electron-electron vertices has thus been obtained in the putative intermediate region. umklapp scattering, though irrelevant in the static limit, was found to be large at finite frequency. This was interpreted as the driving force of a CDW phase gapped in the charge sector, going against the existence of an intermediate metallic state, or at the very least the existence of dominant superconducting correlations whose presence in numerical simulations was attributed to finite-size effects[16,24].

In the first part of this paper, we reexamine this problem using a RG method[25] similar to the fRG and proceed to a detailed scan of the phase diagram of the HH model as extracted from the singularities of susceptibilities and the frequency dependence of electron-electron vertices. We thus reproduce to a high degree of accuracy the boundaries of the intermediate phase found by the QMC simulations of Hardikar *et al.*,[18] at $g_{\rm ph} \gtrsim U$ and arbitrary ω_0[26]. In this sector of the phase diagram, the CDW and to a lesser degree singlet superconducting (SS) response functions are found to be singular. This is compatible with a metallic state characterized by effective attractive couplings, which evolves toward those of the attractive Hubbard model at half-filling when the non adiabatic, $\omega_0 \to \infty$ limit is taken at $U = 0$. The present RG calculations further predict the presence of a particular structure of the boundary between the metallic phase and the M-SDW state. A gapless Luttinger liquid and a gapped $2k_F$ bond-centered charge-density-wave (BOW) phases are successively found to enfold the boundary as a function of U. Both prevent a direct passage from M-SDW to CDW in the $(U, g_{\rm ph})-$plane at finite ω_0.

As to the phase diagram of the PH model at zero temperature, it is known to display a simpler structure. Numerical simulations of the phase diagram from QMC[10] or DMRG[27] techniques for instance agree with a direct transition line between the fully gapped Peierls BOW (P-BOW) state and the M-SDW phase in the $(U, g_{\rm ph})-$plane for small $V \geq 0$, a feature of PH phase diagram also well depicted analytically by the the so-called two-cutoff RG calculations[12,13,28], provided the couplings and Debye frequency ω_D are not too large. The RG calculations to be developed here in the continuum limit agree with QMC results carried out for non dispersive phonons in the weak coupling sector for U and V.[10]

In Sec. II, one-loop flow equations for the scattering amplitudes, self-energy and response functions are given for both models in the electron gas continuum limit. In Sec. III, the flow equations are solved for the HH and PH models, respectively. The singularities in the couplings at zero and finite frequency, along with static susceptibilities are tracked in the $(U, g_{\rm ph})-$plane and serve to map out the phase diagrams for different $\omega_{0,D}$ and V in the case of the PH model. Comparison with numerical results is made. We conclude in Sec. IV.

II. RENORMALIZATION GROUP EQUATIONS OF THE CONTINUUM LIMIT

From the functional integral formulation of the partition function, the integration of the phonon field leads to a (Matsubara) frequency dependent interaction between electrons[25]. When combined with the Coulomb terms U and V, this yields an effective electron-electron interaction of the form:

$$g_{i=1,2,3}(\omega_1, \omega_2, \omega_3) = g_i + \frac{g_{{\rm ph},i}}{1 + (\omega_1 - \omega_3)^2/\omega_{0,D}^2}, \qquad (6)$$

when expressed in the g-ology picture of the electron gas model, where $\omega_i = (2n_i+1)\pi T$. In this continuum framework, the electron spectrum (1) is linearized around the Fermi points $pk_F = \pm k_F$ and becomes

$$\epsilon(k) \approx \epsilon_p(k) = v_F(pk - k_F). \qquad (7)$$

The spectrum is bounded by the band width cutoff, $E_0/2 = \pi v_F/2$, on either side of the Fermi level, where $v_F = 2t$ is the Fermi velocity at half-filling. The interaction defined on the Fermi points then breaks into three pieces, namely the backward (g_1), forward (g_2) and umklapp (g_3) scattering amplitudes whose frequencies satisfy $\omega_1 + \omega_2 = \omega_3 + \omega_4$.

The corresponding attractive amplitudes for the phonon-mediated part are given by

$$g_{\mathrm{ph},1,2,3} = -g_{\mathrm{ph}}, \qquad \text{(HH)} \tag{8}$$

for the HH model, where $g_{\mathrm{ph}} = 2g_0^2/\omega_0$.

For the PH model, however, the electron phonon-matrix element is momentum dependent, which yields

$$g_{\mathrm{ph},1} = -g_{\mathrm{ph},3} = -g_{\mathrm{ph}}; \quad g_{\mathrm{ph},2} = 0, \qquad \text{(PH)}. \tag{9}$$

where

$$g_{\mathrm{ph}} = 2g_D^2/\omega_D. \qquad \text{(PH)}$$

Therefore repulsive umklapp and the absence of forward scattering at the bare level are direct consequences of the momentum dependence of the bond electron-phonon interaction (5). This is a key ingredient for the differences between HH and PH models.

For the Coulomb part that is common to both models, we have the familiar bare coupling combinations of the electron gas at half-filling,[29,30]

$$g_1 = g_3 = U - 2V, \quad g_2 = U + 2V. \tag{10}$$

All the bare amplitudes are confined to the weak-coupling regions $\tilde{g}_i \equiv g_i/\pi v_F < 1$ and $\tilde{g}_{\mathrm{ph}} \equiv g_{\mathrm{ph}}/\pi v_F < 1$.

We apply a Kadanoff-Wilson RG procedure for the partition function,[25,31] which consists at zero temperature of the successive integration of electronic momentum degrees of freedom from the cutoff energy $\pm E_0/2$ down to the energy distance $\pm E_0(\ell)/2$ on either side of the Fermi level. Here $E_0(\ell) = E_0 e^{-\ell}$ is the effective bandwidth at step ℓ. This successive integration in the momentum is performed for all Matsubara frequencies. The frequency axis is divided into 61 sections or patches between the cutoff values $\pm\omega_{\max} = \pm 1.5E_0/2$, which serve as bounds of integration for the frequency. The interactions are taken constant over each patch where the loop integrals are done exactly. The successive integration leads to the flow of coupling constants, one-particle self-energy, and susceptibilities. At the one-loop level, the flow of the normalized scattering amplitudes at $T \to 0$ reads

$$\begin{aligned}
\partial_\ell \tilde{g}_1(\omega_1,\omega_2,\omega_3) &= 2\int_{\omega'} \Big\{ \big[-\tilde{g}_1(\omega_1,\omega',\omega_3)\tilde{g}_1(\omega_4,\omega',\omega_2) - \tilde{g}_3(\omega_1,\omega',\omega_3)\tilde{g}_3(\omega_4,\omega',\omega_2) + \tilde{g}_1(\omega_1,\omega',\omega_3)\tilde{g}_2(\omega',\omega_4,\omega_2) \\
&+ \tilde{g}_3(\omega_1,\omega',\omega_3)\tilde{g}_3(\omega',\omega_4,\omega_2)\big] I_+(\omega',\omega_1-\omega_3) - \tilde{g}_1(\omega_1,\omega_2,\omega')\tilde{g}_2(\omega_3,\omega_4,\omega')I_-(\omega',\omega_1+\omega_2)\Big\}, \qquad (11) \\
\partial_\ell \tilde{g}_2(\omega_1,\omega_2,\omega_3) &= \int_{\omega'} \Big\{ \big[-\tilde{g}_1(\omega_1,\omega_2,\omega')\tilde{g}_1(\omega_3,\omega_4,\omega') - \tilde{g}_2(\omega_1,\omega_2,\omega')\tilde{g}_2(\omega_3,\omega_4,\omega')\big] I_-(\omega',\omega_1+\omega_2) \\
&+ \big[\tilde{g}_2(\omega',\omega_2,\omega_3)\tilde{g}_2(\omega',\omega_4,\omega_1) + \tilde{g}_3(\omega',\omega_2,\omega_3)\tilde{g}_3(\omega',\omega_4,\omega_1)\big] I_+(\omega',\omega_2-\omega_3)\Big\}, \qquad (12) \\
\partial_\ell \tilde{g}_3(\omega_1,\omega_2,\omega_3) &= 2\int_{\omega'} \Big\{ \big[-2\tilde{g}_1(\omega_1,\omega',\omega_3)\tilde{g}_3(\omega_4,\omega',\omega_2) + \tilde{g}_1(\omega_1,\omega',\omega_3)\tilde{g}_3(\omega',\omega_4,\omega_2) \\
&+ \tilde{g}_2(\omega',\omega_4,\omega_2)\tilde{g}_3(\omega_1,\omega',\omega_3)\big] I_+(\omega',\omega_1-\omega_3) + \tilde{g}_2(\omega',\omega_2,\omega_3)\tilde{g}_3(\omega',\omega_4,\omega_1) I_+(\omega',\omega_2-\omega_3)\Big\}, \qquad (13)
\end{aligned}$$

where $\partial_\ell \equiv \partial/\partial\ell$ and $\int_{\omega'} \equiv \int_{-\omega_{\max}}^{+\omega_{\max}} d\omega'/2\pi$. Here $I_\mp$ refer to the $2k_F$ electron-hole (Peierls) and electron-electron (Cooper) loops,

$$I_\mp(\omega,\Omega) = \Lambda_\ell \frac{(\omega - \Sigma(\omega))(\omega \mp \Omega \pm \Sigma(\Omega \pm \omega)) + \Lambda_\ell^2}{[(\omega - \Sigma(\omega))^2 + \Lambda_\ell^2][(\omega \mp \Omega \pm \Sigma(\Omega \pm \omega))^2 + \Lambda_\ell^2]}, \tag{14}$$

where $\Lambda_\ell = E_0(\ell)/2$. The imaginary part of the Matsubara self-energy, Σ, for right or left-going electrons obeys the equation

$$\partial_\ell \Sigma(\omega) = \int_{\omega'} \Big\{ \tilde{g}_1(\omega',\omega,\omega_1) - 2\tilde{g}_2(\omega,\omega',\omega) \Big\} \times \Lambda_\ell \frac{\omega' - \Sigma(\omega')}{[\omega' - \Sigma(\omega')]^2 + \Lambda_\ell^2}, \tag{15}$$

with the initial condition $\Sigma(\omega)|_{\ell=0} = 0$. The one-loop flow is essentially governed by the superimposition of Cooper and Peierls pairing channels which interfere with one another, mixing ladder, closed loop, and vertex correction diagrams at every order. The combination controls the nature of correlation at long distance, and in the presence of a phonon part will be dependent on the degree of retardation or the phonon frequency $\omega_{0,D}$.

The nature of correlations as a function of ℓ are analyzed from a selected set of static normalized susceptibilities $\tilde{\chi}_\mu (\equiv \pi v_F \chi_\mu)$, namely those likely to be singular in the density-wave and superconducting channels. The

static susceptibilities obey an equation of the form

$$\partial_\ell \tilde{\chi}_\mu \;=\; \int_\omega |z_\mu(\omega)|^2 I_\mp(\omega,0). \tag{16}$$

Each of these involves a pair vertex function z_μ governed by the equation

$$\partial_\ell\, z_\mu(\omega) = \int_{\omega'} \tilde{g}_\mu(\omega',\omega,\omega) z_\mu(\omega') I_\mp(\omega',0), \tag{17}$$

where $z_\mu(\omega)|_{\ell=0} = 1$. For the charge density-wave channel, we shall consider the CDW and BOW susceptibilities at the wave vector $2k_F$, and to which correspond the combinations of couplings

$$\tilde{g}_\mu(\omega',\omega,\omega)\Big|_{\mu=\mathrm{CDW(BOW)}} = \tilde{g}_2(\omega',\omega,\omega) - 2\tilde{g}_1(\omega,\omega',\omega) \pm\; [\tilde{g}_3(\omega,\omega',\omega') - 2\tilde{g}_3(\omega',\omega,\omega')]. \tag{18}$$

For the spin-density-wave channel, the antiferromagnetic or site centered SDW susceptibility may be also singular; it corresponds to the combination of couplings

$$\tilde{g}_{\mu=\mathrm{SDW}}(\omega',\omega,\omega) \;=\; \tilde{g}_2(\omega',\omega,\omega) - [\tilde{g}_3(\omega,\omega',\omega') - 2\tilde{g}_3(\omega',\omega,\omega')]. \tag{19}$$

In the superconducting channel, only the SS susceptibility may develop a singularity. It is linked to the combination,

$$\tilde{g}_{\mathrm{SS}}(\omega',\omega,\omega) = -\tilde{g}_2(\omega,-\omega,\omega') - \tilde{g}_1(-\omega,\omega,\omega'). \tag{20}$$

The solution of equations as a function of ℓ for χ_μ and the scattering amplitudes reveals the singularities in χ_μ; these allow the identification of dominant and subdominant singular correlations[25]. A divergence at a finite ℓ_c indicates the breakdown of the weak-coupling one-loop RG procedure. Nevertheless, it singles out an energy scale or a gap $\Delta = E_F e^{-\ell_c}$ at zero temperature that correlates with a gap in the spin or/and charge degrees of freedom at ℓ_c. The gap in the spin sector is associated with a singularity in the static, $\omega \to 0$, limit for the attractive backward-scattering amplitude (11), whereas in the charge sector, a gap is found for singular either static repulsive or attractive umklapp (13).

III. RESULTS AND DISCUSSION

A. Holstein-Hubbard model

Let us first consider the HH model at $U > 0$. In Fig. 1 typical ℓ dependencies for the susceptibilities are shown for a fixed bare phonon-mediated coupling amplitude, $g_{\mathrm{ph}} = 2t$, and phonon frequency $\omega_0 = t$. At $U = 0.5t$, that is in the region well above the bisecting line $g_{\mathrm{ph}} = U$, a divergence is found only for the CDW

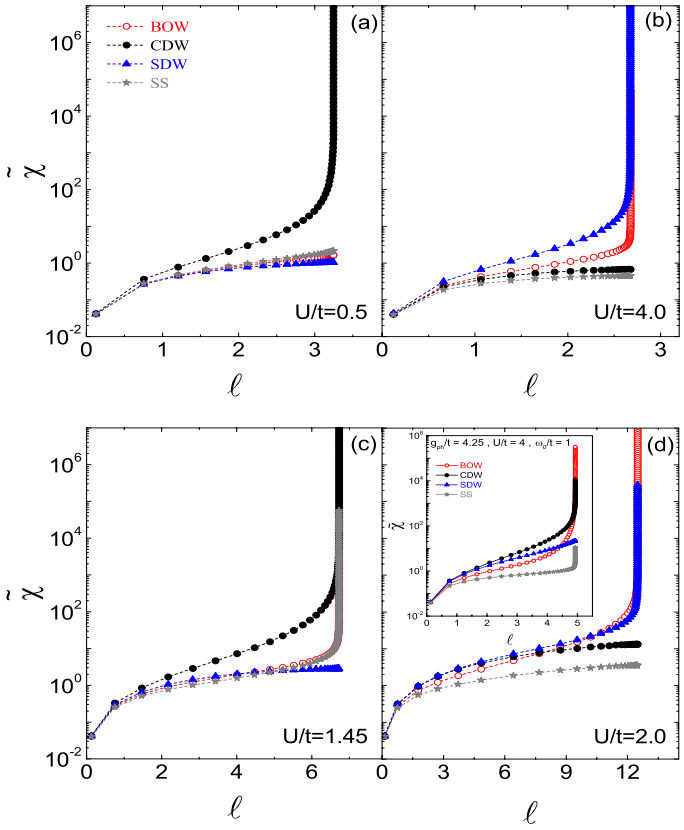

FIG. 1: (Color online) In (a)-(c), the flow of normalized susceptibilities $\tilde{\chi}_\mu$ *vs* ℓ for the Holstein-Hubbard model for $g_{\mathrm{ph}}/t = 2$ at different values of U/t. In (d), the flow of susceptibilities on the boundary of spin-density-wave phase with the intermediate phase; insert: susceptibilities on the boundary with the charge-density-wave phase. In all cases the phonon frequency is fixed at $\omega_0 = t$.

susceptibility [Fig. 1 (a)]. The value of $\ell_c \simeq 3.25$ extracted from the Fig. 1 (a) leads to a one-loop CDW gap $\Delta = E_F e^{-\ell_c}$ that is sizably reduced compared to the adiabatic –mean field– value[25] $\Delta_0 = E_F e^{-1/(2\tilde{g}_{\mathrm{ph}})}$, of the pure phonon model at $\omega_0 \to 0$ and for which, $\ell_0 = \pi/2$ at the coupling considered here. The value of Δ is also smaller but closer to the non adiabatic $\omega_0 \to \infty$ limit of Eqs. (11-13) at $U = 0$, corresponding to an effective attractive Hubbard model, where $\Delta_\infty = E_F e^{-1/\tilde{g}_{\mathrm{ph}}}$ and $\ell_\infty = \pi < \ell_c$ at the one-loop level[29]. Repulsive U, which primarily reduces double occupancy of electrons on sites decreases CDW correlations and in turn their coupling to $2k_F$ molecular phonons through vertex corrections in Eqs. (11)–(13), can explain these downward shifts of the gap[12,13].

Regarding now the structure of scattering amplitudes at finite frequency in this CDW phase, we follow Ref.[19] and show in Fig. 2 (a) the contour plot of the projected $\tilde{g}_{i=1,2,3}(\omega_1,\omega_2,\omega_3)$ in the (ω_1,ω_2)-plane when $\ell \approx \ell_c$. As previously noted in the framework of fRG[19], the scattering amplitudes display significant structure as a function of frequency, notably an attractive singular behavior for

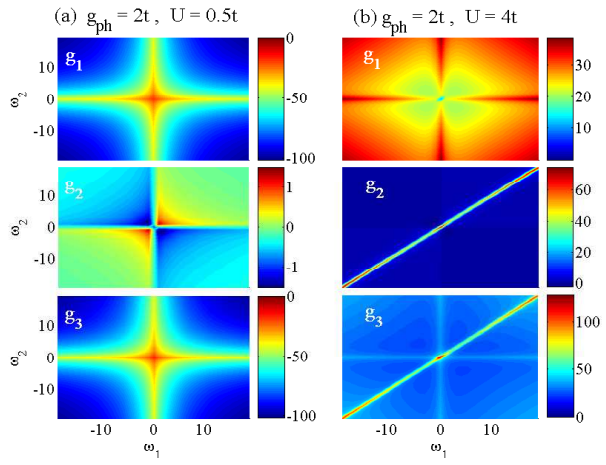

FIG. 2: (Color online) Contour plot of the frequency dependent normalized couplings $\tilde{g}_i(\omega_1, \omega_2, \omega_1)$ in a finite portion of the (ω_1, ω_2) plane at $g_{\rm ph} = 2t$, $\omega_0 = t$, ℓ close to the critical ℓ_c, and for two values of Coulomb interaction: (a) $U = 0.5t$ (CDW) and (b) $U = 4t$ (M-SDW).

the CDW phase that persists away from the origin of the (ω_1, ω_2)-plane. Divergences toward negative values are seen in both $g_1(\omega_1, \omega_2, \omega_1)$ and $g_3(\omega_1, \omega_2, \omega_1)$ with maxima at the origin [Fig. 2 (a)], supporting the existence of a gap in both spin and charge degrees of freedom compatible with the absence of enhancement in spin correlations and the existence of commensurate CDW order at half-filling.

One can wonder about the impact of vertex singularities in the finite frequency range on correlations. In the present RG procedure both the marginal and irrelevant (frequency) parts of couplings are comprised in the three-variables scattering amplitudes $g_i(\omega_1, \omega_2, \omega_3)$. However, one can get a rough idea of how the frequency dependence emerges. Assuming that the amplitudes can be expanded around the origin as

$$g_i(\omega_1, \omega_2, \omega_3) = g_i(0,0,0) + \sum_{j=1}^{3} \bar{g}_{i,j} \omega_j^2 + \ldots ,$$

we see that the amplitudes, $\bar{g}_{i,j}$, etc., of the frequency dependent part are by power counting superficially irrelevant in the RG sense. However, these will be coupled to the marginally relevant $g_i(0,0,0)$ at the one-loop level and may become in turn relevant when one or more $g_i(0,0,0)$ scales to strong coupling, that is as ℓ approaches ℓ_c. This is likely what happens in the present RG procedure. Being strongly weakened by the frequency convolution of couplings and single loops (Peierls and Cooper) which decay as ω^{-2} [Eqs. (14) and (17)], these high frequency singularities have in the end a limited impact on susceptibilities and then correlations; the corrections remaining in most cases at a quantitative level. In special regions of the phase diagram, however, the consequence can be more substantial and can act on the nature of the ground state as will be discussed below.

If we now move on the opposite side of the bisecting line, on the Hubbard side of the phase diagram at $U = 4t$, the strongest singularity is found for the SDW susceptibility at $\ell_c \simeq 2.7$, which comes with subdominant singular BOW correlations [Fig. 1 (b)]. These are the characteristics of the repulsive Hubbard model at half-filling which presents a charge or Mott gap Δ at ℓ_c, in accord with singular repulsive $g_2(0,0,0)$ and umklapp $g_3(0,0,0)$ scatterings at zero frequency as meant in Fig. 2 (b). As for the backscattering, the same Figure shows that it becomes repulsive and large close to ℓ_c over the whole frequency range, with only a minimum for $g_1(0,0,0)$ [$\ll g_{2,3}(0,0,0)$]. Nevertheless, relevant repulsive backscattering introduced by the dynamics leaves the spin sector gapless as shown by the singular behavior of the SDW response in Fig. 1 (b). One also notes that the strong repulsive coupling that characterizes the backscattering amplitude $g_1(\omega_1, \omega_2, \omega_3)$ at finite frequency has a limited influence on correlations, reducing for example the amplitude of BOW correlations compared to the situation of the pure Hubbard model.

Regarding the amplitude of the gap, the finite attractive contribution coming from phonons [Eq. (8)] weakens the amplitude of Δ compared to the pure Hubbard result[29], $\Delta_\rho = E_F e^{-1/\tilde{U}}$, which yields $\ell_\rho = \pi/2 < \ell_c$, at $U = 4t$.

1. *Intermbehaviorediate phase*

As a function of U, the ground state evolves from the fully gapped CDW to the M-SDW states discussed above. Within the CDW state the reduction of the gap Δ with U carries on up to a critical value where static umklapp, $g_3(0,0,0)$, is no longer singular, but goes to zero and becomes irrelevant (Fig. 3)[8,19], whereas $g_1(0,0,0)$ and $g_2(0,0,0)$ remain attractive as in Fig. 2 (a). The irrelevance of the static g_3 is concomitant with the onset of an additional, but subdominant singular susceptibility in the SS channel, as shown in Fig. 1 (c). From the same figure, we also note that the BOW response is also enhanced. The CDW-SS singular correlations persist over a finite U-interval before the system ultimately enters in the M-SDW phase described above [Fig. 1 (b)]. A detailed scan in the $(U, g_{\rm ph})$-plane allows us to outline an entire intermediate (I) region of the phase diagram of Fig. 2 (b) where similar features for CDW and SS cor-

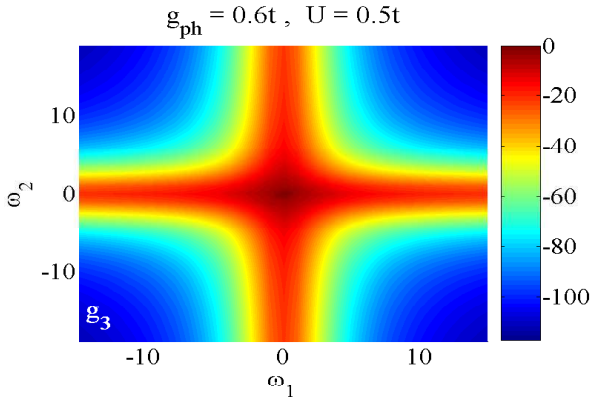

FIG. 3: (Color online) Typical contour plot of umklapp scattering amplitude $g_3(\omega_1, \omega_2, \omega_1)$ in the (ω_1, ω_2)-plane close to ℓ_c in the intermediate I-phase at $\omega_0 = t$.

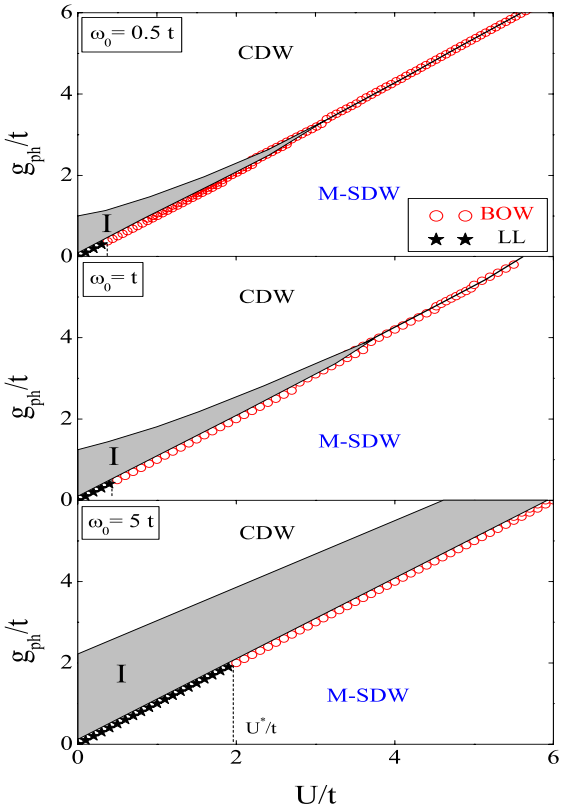

FIG. 4: (Color online) One-loop RG phase diagram of the 1D Holstein-Hubbard model at different molecular phonon frequencies: $\omega_0 = 0.5t$ (a), $\omega_0 = t$ (b) and $\omega_0 = 5t$ (c).

relations are found. Note that within the I region, we observe a reinforcement of the SS correlations as U/t decreases; its singular behavior reaching the CDW one as $U \to 0$ and $\omega_0 \gg t$, which is essentially the situation of the attractive Hubbard model.

The boundary of the I state closes at some point $(U^c, g^c_{\rm ph})$, whose locus depends on the phonon frequency ω_0. The resulting phase diagrams shown in Fig. 4 for different ω_0 stand particularly well the comparison with previous numerical analysis, notably those carried out by the QMC[18] and DMRG[17] methods. Comparing for instance the metallic I region obtained from the QMC simulations of Hardikar and Clay (see Fig. 8 of Ref.[18]) with the one deduced here by RG, a quite accurate match is found for an amazing range of interactions and phonon frequencies.

As to the the origin of the I phase, it must be stressed at the outset that within the electron gas model, irrelevant umklapp and strong attractive backward scattering, along with degenerate CDW and SC singular susceptibilities, are well known characteristics of the attractive 1D Hubbard model at half filling[29,30,32]. For the HH model, this limit is clearly realized at $U = 0$, along the $g_{\rm ph}$ axis as $\omega_0 \to \infty$ (see note in Ref.[26]). As ω_0 is increased beyond t, Fig. 4 shows indeed an ever-growing I region which includes the $(0, g_{\rm ph})$ axis. This suggests that the whole region is governed by a Luther-Emery type of fixed point[29,33], characterized by effective attractive couplings and a gap in the spin sector, despite finite retardation and repulsive U[34]. Both split the degeneracy between CDW and SS correlations reinforcing the former with respect to the latter. According to the combination of couplings (18) for CDW susceptibility, singular attractive umklapp scattering at finite frequency does have an impact, thought limited, in favoring an increase of CDW correlations and lack of degeneracy between CDW and SS in the I region [Fig. 1 (c)].

The above results are compatible with those previously found from fRG by Tam *et al.*[19] for selected points of the phase diagram well outside and inside the supposed I region. A different view was held, however, as to the properties of charge degrees of freedom in this specific part of the phase diagram. The presence of singular and negative umklapp scattering at finite frequency found in the I region (Fig. 3), was interpreted as the driving force of the CDW state, whose charge sector was then considered still gapped and insulating. We consider that a spatially uniform charge gapped state, if it exists, must be manifest in the equilibrium –static– properties rather than in the dynamics. Otherwise the Mott-insulating state thus obtained would be hard to reconcile with a finite charge compressibility,[18] and singular superconducting correlations.

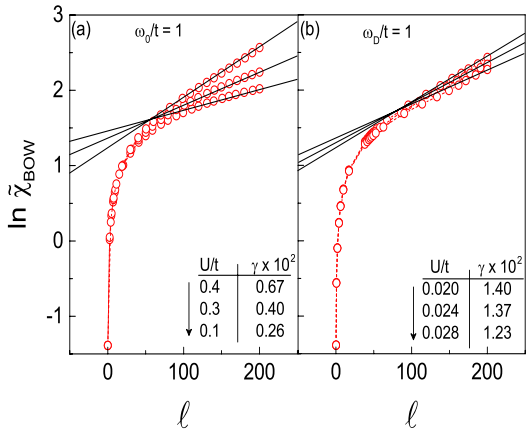

FIG. 5: (Color online) The power-law behavior $\chi_{\rm BOW} \sim [E_0(\ell)]^{-\gamma}$ (straight lines) of the BOW susceptibility on the LL line of the phase diagram at different U for the HH model in (a) [Fig. 4 (b)], and for the PH model in (b) [Fig. 9 (c)]. In both cases, $\omega_0/t = 1$.

2. *Structure of the phase boundary*

We close this subsection by a detailed examination of the boundary to the M-SDW state in the phase diagram. As one moves along the bisecting line, $g_{\rm ph} = U$, the RG calculations reveal the existence of a gapless transition line between the M-SDW and I phases (Fig. 4). At small U along this line, no singularity is encountered at finite ℓ in the susceptibilities. These rather exhibit a power law singularity of the form $\tilde{\chi} \sim [E_0(\ell)]^{-\gamma}$ at large ℓ as shown in Fig. 5 (a). The exponent γ is non universal, thought very small and positive, and is the largest for the BOW susceptibility. Within one-loop approximation, such a power law is characteristic of a Luttinger liquid (LL) with effective very weak repulsive interactions at low energy. This is confirmed by the contour plots of Fig. 6 for the couplings in the (ω_1, ω_2) plane, where at large ℓ all the couplings are vanishingly small at the origin and remain weak at finite frequency. The LL line terminates on the bisecting line at the finite value $U^* = g^*_{\rm ph}$, which increases with ω_0 (Fig. 4). It has been checked that in the limit of large ω_0, the LL and $U = g_{\rm ph}$ lines merge over the entire range of couplings with $\gamma \to 0$, consistently with vanishing initial couplings in (6). It is worth noting that the existence of a LL metallic phase with a similar ω_0 dependence, albeit on a larger area of the phase diagram has been already pointed out by Fehske *et al.*[20] using the DMRG technique, thought constrained by possible finite-size effects.

Another feature emerges at finite ω_0 where the ending point $(U^*, g^*_{\rm ph})$ in Fig. 4 marks the beginning of a different boundary with the M-SDW phase. For $U > U^*$ a singularity appears in the susceptibilities at finite ℓ_c, the strongest being for BOW, whereas SDW correlations become subdominant [Fig. 1 (d)]; no enhancement in

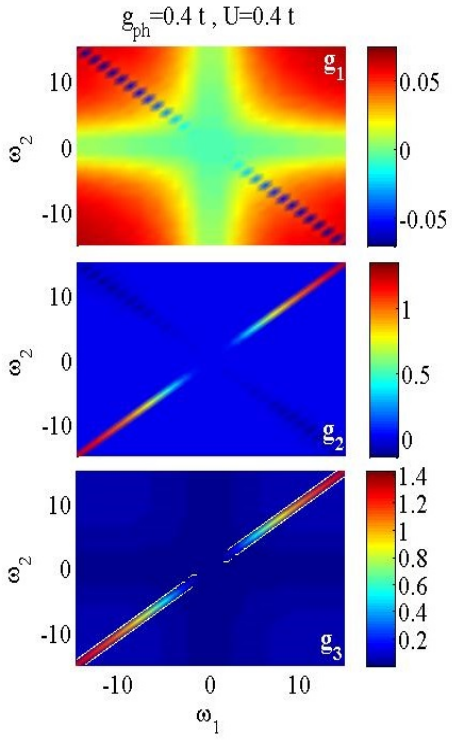

FIG. 6: (Color online) Contour plots of the scattering amplitudes $g_i(\omega_1, \omega_2, \omega_1)$ in the (ω_1, ω_2)-plane at large ℓ and $\omega_0 = t$ for the metallic Luttinger liquid (LL) line of the HH model.

CDW correlations is found. Actually, as one hits the boundary from below the relative importance of SDW and BOW correlations is inverted compared to the M-SDW phase [see Figs. 1 (b), (d)]. The frequency profile of coupling constants in this BOW phase along the boundary is of interest. For small $g_{\rm ph}/t$ and finite ω_0, as shown in Fig. 7 (a), both $g_2(0,0,0)$ and $g_3(0,0,0)$ scale to strong repulsive coupling as $\ell \to \ell_c$, which is indicative of a charge gap. However, $g_1(\omega_1, \omega_2, \omega_1)$ remains relatively small, although *attractive* at zero frequency and its close vicinity. It is from these frequency effects, a consequence of retardation, that comes the origin of dominant BOW correlations. According to the combination of couplings for the BOW susceptibility in Eq. (18), a change of sign in the backscattering in the low frequency range is sufficient to reinforce BOW correlations against SDW [Eq. (20)].

As $g_{\rm ph}/t$ and U become larger at finite ω_0 along the boundary, $g_1(\omega_1, \omega_2, \omega_1)$ develops much stronger attraction at the origin and beyond, suggesting the presence of a spin gap at ℓ_c. This is reflected by the absence of singular SDW correlations in Fig. 1 (d) (insert). While $g_2(0,0,0)$ becomes small as shown in Fig. 7 (b), g_3 remains positive at the origin and its neighbourhood, which indicates that at sizable $g_{\rm ph}$ the BOW order is now gapped in the spin sector and prevails over CDW that also becomes singular on the boundary. By cranking up further $g_{\rm ph}/t$ at finite ω_0 along the boundary, namely beyond the limitations of the RG, it is likely that BOW

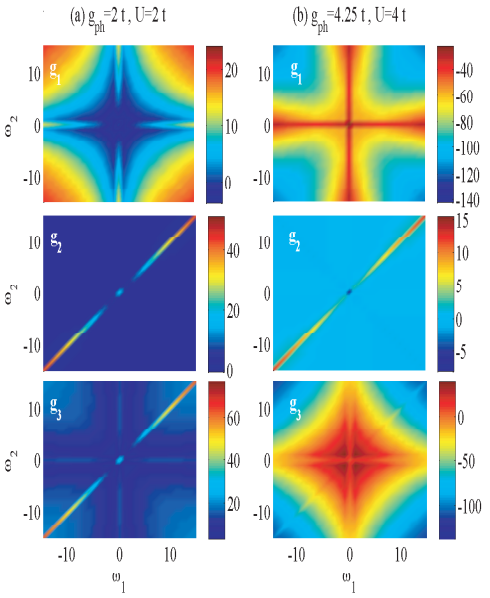

FIG. 7: (Color online) Contour plots of the scattering amplitudes $g_i(\omega_1,\omega_2,\omega_1)$ in the (ω_1,ω_2)-plane for the HH model in the BOW regime of the boundary with the intermediate phase at small U (a) and with the CDW phase at larger U (b).

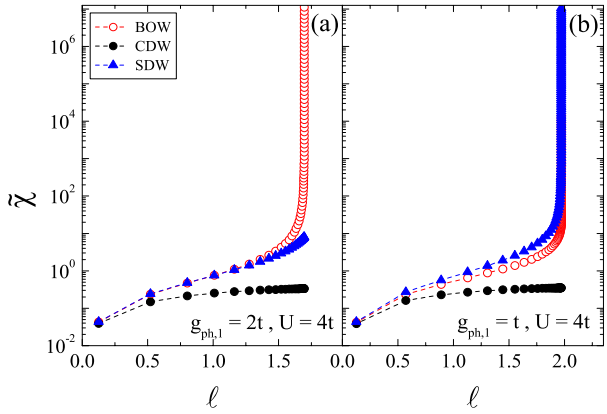

FIG. 8: (Color online) Selected susceptibilities versus ℓ in the P-BOW (a) and M-SDW (b) parts of the phase diagram of the Peierls-Hubbard model of Fig. 9 (a) at $\omega_D = t$.

would be suppressed and the system would evolve toward a CDW ground state. The BOW phase emerging in this part of the CDW–M–SDW boundary, as a consequence of retardation at finite ω_0, is reminiscent of the repulsive 1D extended Hubbard lattice model where the BOW phase is known to enfold the $U = 2V$ line[35]. This separatrix is known to separate the same CDW and M-SDW ground states in the continuum approximation[29]. The 1D extended Hubbard model being defined on a lattice, however, it is the *momentum dependence* of couplings, though irrelevant in the RG sense, that break the CDW−M-SDW degeneracy in favor of a BOW state[36,37].

B. Peierls-Hubbard model

1. *V=0 case*

We now examine the PH model at finite repulsive U. As mentioned in Sec. II, the coupling of electronic bond transfer to acoustic phonons introduces particular initial conditions for the phonon-mediated contribution to couplings of the PH model in (9). Only the phonon induced backscattering is attractive, whereas the umklapp term, like U, is repulsive. According to (18), such a combination clearly favours the occurrence of the Peierls BOW (P-BOW) phase against CDW whose enhancement is totally absent across the $(U, g_{\rm ph})-$plane. As shown in Fig. 8, either a BOW or a SDW singularity is found at finite $g_{\rm ph}$, as a function of U; their tracking at $V = 0$ yields the phase diagram of Fig. 9 (top) at different Debye frequencies.

On the P-BOW side, the gap amplitude $\Delta = E_F e^{-\ell_c}$ extracted at ℓ_c [Fig. 8 (a)], is always larger than the $U = 0$ adiabatic mean-field value, $\Delta_0 = E_F e^{-1/2\tilde{g}_{\rm ph}}$. Finite U enhances BOW correlations and then strengthens their coupling to $2k_F$ phonons in Eqs. (11-13)[12,13]. The enhancement of the Peierls order parameter by repulsive U is a well-known result of early numerical simulations on that model[4,5]. Regarding the scattering amplitudes, singularity of $g_1(0,0,0)$ is found in the attractive sector, while the strong-coupling peaks of both $g_2(0,0,0)$ and umklapp $g_3(0,0,0)$ are for positive values (Fig. 10). These are indicative of a fully gapped phase, as expected for the commensurate Peierls order at half-filling. The frequency dependence of the $g_i(\omega_1,\omega_2,\omega_1)$ displays similar features over the whole P-BOW region. However, the influence of strong coupling at finite frequency on correlations remains weak.

The transition line between P-BOW and M-SDW states in the phase diagram is also of interest. Owing to the reinforcement of electronic BOW correlations by U, the transition to the M-SDW line occurs below the bisecting line $g_{\rm ph} = U$, in contrast to what has been obtained for the HH model (Fig. 2). As a result, moving toward the adiabatic limit for small ω_D the P-BOW phase grows in importance to the detriment of M-SDW. In Fig. 9 (bottom), we have plotted the phonon coupling parameter $\alpha[\equiv (g_{\rm ph}\omega_D/8t^2)^{1/2}]$ versus U for the transition line[10]. The trace fits fairly well the power-law $\alpha_c \sim U^\eta$, with the exponent $\eta \simeq 0.31$ at $V = 0$. Similar algebraic variation has been reported by QMC simulations at finite V[10] (see Sec. III B 2). For most $g_{\rm ph}$ values, the line $\alpha_c(U)$ shows a direct transition between the P-BOW and M-SDW phases [Fig. 9 (top)], except for very small $g_{\rm ph}$, where there is a finite but minute U interval in which LL metallic conditions prevail (see insets of Fig. 9). As in the HH model, a power-law dependences of the BOW susceptibility is found, as shown in Fig. 5 (b). Otherwise, due

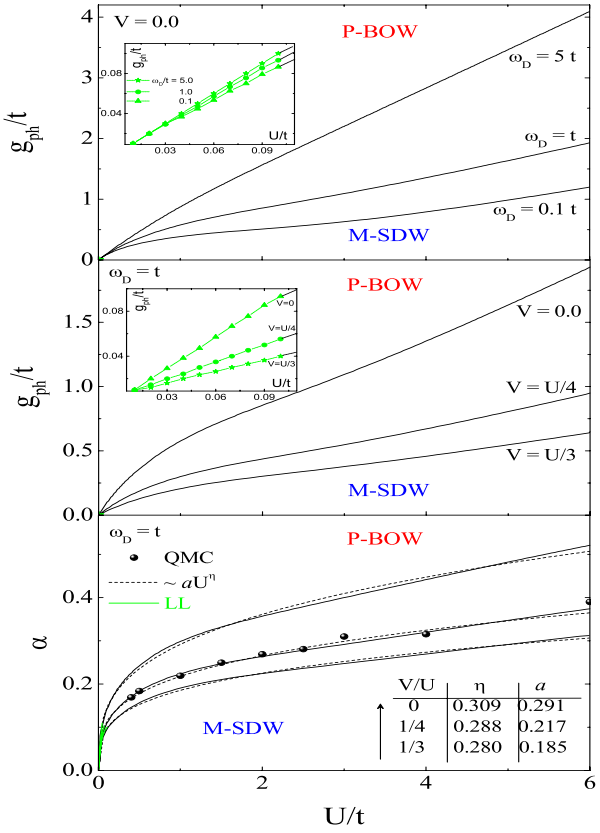

FIG. 9: (Color online) Phase diagram of the PH model for (top) $\omega_D/t = 0.1, 1$, and 5 at $V = 0$; (middle) $\omega_D/t = 1$ and $V \geq 0$ (inserts: zoom of the Luttinger liquid line at very small couplings); (bottom) comparison with a power law dependence of the boundary line between P-BOW and M-SDW (dashed lines) for different values of V (bottom). The full circles are the QMC results of Ref.[10].

to the fact that for the PH model both the Coulomb and phonon-induced terms contribute positively to umklapp scattering [Eqs. (9) and (10)], the charge sector is gapped and the conditions for the emergence of an intermediate metallic phase are not satisfied.

As to the M-SDW phase at sufficiently strong U, their characteristics are similar to the one found for the HH model. This is confirmed by the frequency profiles of scattering amplitudes of Fig. 10 (b) close to ℓ_c, when compared to those of Fig. 2 (b). The backscattering amplitude develop sizable repulsive values with a minimum for $g_1(0,0,0)$, subordinated to the singular positive peaks $g_2(0,0,0)$ and $g_3(0,0,0)$ at positive values. The Mott gap is associated with the strongest singularity in $\chi_{\rm SDW}$ at ℓ_c closely followed by $\chi_{\rm BOW}$, as shown in Fig. 8 (b).

2. *Finite V*

We close the section by examining the influence of small nearest-neighbor repulsion V on the structure of

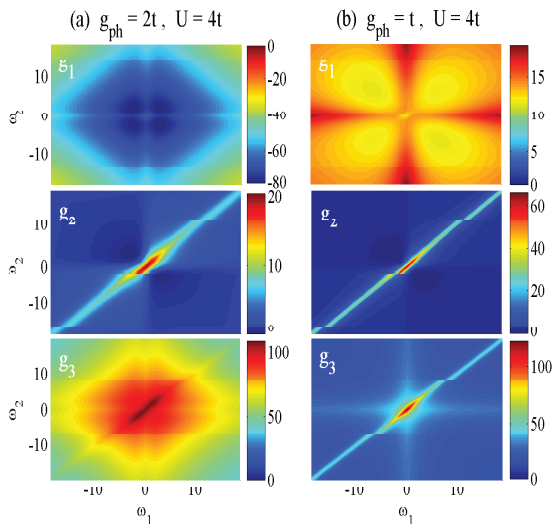

FIG. 10: (Color online) Contour plot of the scattering amplitudes $g_i(\omega_1, \omega_2, \omega_1)$ in the (ω_1, ω_2)-plane for the Peierls Hubbard phase diagram of Fig. 9 (top) close to ℓ_c and at $\omega_D = t$: (a), the P-BOW phase and (b), the M-SDW phase.

the phase diagram of the PH model. In Fig. 9 (middle), the critical line $\alpha_c(U)$ is plotted for different V ($< U/2$). We first observe that the P-BOW region increases in size with V, as described by the fit to the expression $\alpha_c = aU^\eta$ showing a drop of the coefficient a and a power-law exponent η which depends on the value of V. The reinforcement of BOW correlations and in turn of the Peierls state follows from the decrease (increase) of g_1 (g_2) by V in Eq. (10), which compensates the drop in umklapp and then according to (18) makes the BOW correlations and its coupling to phonons larger. The frequency dependence of the $g_i(\omega_1, \omega_2, \omega_1)$ projected in the (ω_1, ω_2)-plane present essentially the same characteristics as those obtained in the Hubbard case for $V = 0$ (Fig. 10).

The results obtained at $V = U/4$ can be compared to QMC simulations performed in the same model conditions.[10] As shown in Fig. 9 (bottom), the power law found by QMC for α_c is fairly well reproduced by the RG method over the whole interval of acceptable couplings for a weak coupling scheme.

IV. SUMMARY AND CONCLUDING REMARKS

Summarizing, we have studied the phase diagrams of 1D Holstein-Hubbard and Peierls-Hubbard models at half filling by a weak-coupling RG method. The (U,$g_{\rm ph}$) phase diagrams that are mapped out from the susceptibilities and frequency-dependent scattering amplitudes at the one-loop level adhere for the most part to the results

of numerical simulations, in particular those of quantum Monte Carlo methods for which the most detailed studies have been carried out and the best comparison can be established in weak coupling.

In the case of the Holstein-Hubbard model, the RG results pinpoint a precise delimitation of an intermediate region separating the commensurate CDW and a Mott-insulating SDW phases in the phase diagram. The singular static superconducting correlations found throughout this region, though always subordinate to CDW and tied to irrelevant umklapp scattering at zero frequency, are congruent with the metallic character of this region. The present results also revealed an internal structure of the phase boundary with the M-SDW phase with the presence of distinct phases, unanticipated and unexplored from the viewpoint of previous works on this model. A very weakly correlated Luttinger liquid followed by a BOW phase characterized by either a charge or spin gap has been found depending on the strength of the Coulomb term. The BOW phase replaces the Mott-SDW state as a result of retardation, whose dynamics generates an attraction in the backscattering amplitude alone, in analogy with momentum-dependent effects for the appearance of the BOW phase enfolding the $U = 2V$ line of the 1D extended Hubbard lattice model.

A similar analysis carried out on the Peierls-Hubbard model with its peculiar momentum- and frequency-dependent scattering amplitudes rather reveals a Mott SDW state competing with the Peierls-BOW order whose prominence in the phase diagram grows as a function of retardation, and intrasite and inter site Coulomb terms U and V. The nearly structureless boundary between the two ground states in the $(U, g_{\rm ph})-$plane of the phase diagram follows a power-law profile compatible with numerical simulations.

Acknowledgments

C. B thanks Martin Hohenadler for discussions on several aspects of this work. The financial support of the National Science and Engineering Research Council of Canada (NSERC) and the Réseau Québécois des Matériaux de Pointe (RQMP) is also acknowledged. Computational resources were provided by RQCHP and Compute Canada.

* Electronic address: hassan.bakrim@USherbrooke.ca
† Electronic address: claude.bourbonnais@USherbrooke.ca

[1] J. P. Pouget, Crystals **2**, 466 (2012); Physica B (2014), in press.
[2] O. Gurnnasson and O. Röuch, J. Phys.: Condens. Matter **20**, 043201 (2008).
[3] M. Capone, C. Castellani, and M. Grilli, Adv. Condens. Matter Phys. **2010**, 920860 (2010).
[4] J. E. Hirsch, Phys. Rev. Lett. **51**, 296 (1983).
[5] S. Mazumdar and S. N. Dixit, Phys. Rev. Lett. **51**, 292 (1983).
[6] H. Bakrim and C. Bourbonnais, Phys. Rev. B **90**, 125119 (2014).
[7] T. Holstein, Ann. Phys. **8**, 325 (1959).
[8] J. E. Hirsch, Phys. Rev. B. **31**, 6022 (1985).
[9] W. P. Su, J. R. Schrieffer, and A. J. Heeger, Phys. Rev. Lett. **42**, 1698 (1979), see also S. Barisic, Phys. Rev. B **5**, 932 (1972).
[10] P. Sengupta, A. W. Sandvik, and D. K. Campbell, Phys. Rev. B **67**, 245103 (2003).
[11] F. Guinea, J. Phys. C: Solid State Phys. **16**, 4405 (1983).
[12] L. G. Caron and C. Bourbonnais, Phys. Rev. B **29**, 4230 (1984).
[13] I. P. Bindloss, Phys. Rev. B **71**, 205113 (2005).
[14] E. Jeckelmann, C. Zhang, and S. R. White, Phys. Rev. B **60**, 7950 (1999).
[15] Y. Takada and A. Chatterjee, Phys. Rev. B **67**, 081102(R) (2003).
[16] R. T. Clay and R. P. Hardikar, Phys. Rev. Lett. **95**, 096401 (2005).
[17] M. Tezuka, R. Arita, and H. Aoki, Phys. Rev. Lett. **95**, 226401 (2005).
[18] R. P. Hardikar and R. T. Clay, Phys. Rev. B **75**, 245103 (2007).
[19] K.-M. Tam, S.-W. Tsai, D. K. Campbell, and A. H. C. Neto, Phys. Rev. B **75**, 161103(R) (2007).
[20] H. Fehske, G. Hager, and E. Jeckelmann, Eur. Phys. Lett. **84**, 57001 (2008).
[21] A. Payeur and D. Sénéchal, Phys. Rev. B **83**, 033104 (2011).
[22] M. Hohenadler and F. F. Assaad, Phys. Rev. B **87**, 075149 (2013).
[23] M. Tezuka, R. Arita, and H. Aoki, Phys. Rev. B **76**, 155114 (2007).
[24] K.-M. Tam, S.-W. Tsai, and D. K. Campbell, Phys. Rev. B **84**, 165123 (2011).
[25] H. Bakrim and C. Bourbonnais, Phys. Rev. B **76**, 195115 (2007).
[26] In reference[25] where the same RG technique has been used for the purely Holstein limit at $U = 0$, no singular superconducting correlations were found besides the dominant charge-density-wave ones. This was due to the range of couplings $g_{\rm ph}$ and frequency ω_0 used in that work which lies above the intermediate region in the phase diagram.
[27] C. J. Pearson, W. Barford, and R. J. Bursill, Phys. Rev. B **83**, 195105 (2011).
[28] G. T. Zimanyi, S. A. Kivelson, and A. Luther, Phys. Rev. Lett. **60**, 2089 (1988).
[29] V. J. Emery, in *Highly Conducting One-Dimensional Solids*, edited by J. T. Devreese, R. E. Evrard, and V. E. van Doren (Plenum, New York, 1979), p. 247.
[30] J. Solyom, Adv. Phys. **28**, 201 (1979).
[31] C. Bourbonnais and L. G. Caron, Int. J. Mod. Phys. B **05**, 1033 (1991).
[32] T. Giamarchi, *Quantum Physics in One Dimension* (Oxford University Press, Oxford, 2004).

[33] J. Voit, Rep. Prog. Phys. **58**, 977 (1995).
[34] M. Hohenadler *et al.,* unpublished results.
[35] A. W. Sandvik, L. Balents, and D. K. Campbell, Phys. Rev. Lett. **92**, 236401 (2004).
[36] K.-M. Tam, S.-W. Tsai, and D. K. Campbell, Phys. Rev. Lett. **96**, 036408 (2006).
[37] M. Ménard and C. Bourbonnais, Phys. Rev. B **83**, 075111 (2011).